CrystEngComm

From Light to Heavy Alkali Metal Tetraphosphonates (M = Li, Na, K, Rb, Cs): Cation Size-Induced Structural Diversity and Water-Facilitated Proton Conductivity

Journal:	*CrystEngComm*
Manuscript ID	CE-ART-08-2018-001351.R1
Article Type:	Paper
Date Submitted by the Author:	14-Sep-2018

Complete List of Authors:	Demadis, Konstantinos; University of Crete, Department of Chemistry Salcedo, Inés; Universidad de Malaga Facultad de Ciencias Colodrero, Rosario; Universidad de Malaga, Departamento de Quimica Inorganica, Cristalografia y Mineralogia; University of Wolverhampton, Faculty of Science and Engineering Papadaki, Maria; University of Crete, Department of Chemistry Vasileiou, Antonia; University of Crete, Department of Chemistry Losilla, Enrique; Universidad de Malaga, Quimica Inorganica Pascual, Olivera-Pastor; Universidad de Malaga, Departamento de Quimica Inorganica, Cristalografia y Mineralogia Cabeza Díaz, Aurelio; Universidad de Malaga, Departamento de Quimica Inorganica, Cristalografia y Mineralogia Bazaga García, Montse; Universidad de Malaga Infantes-Molina, Antonia; Instituto de Catálisis y Petroleoquímica, CSIC; University of Málaga, Inorganic Chemistry Mezei, Gellert; Western Michigan University, Chemistry

Journal Name

ARTICLE

From Light to Heavy Alkali Metal Tetraphosphonates (M = Li, Na, K, Rb, Cs): Cation Size-Induced Structural Diversity and Water-Facilitated Proton Conductivity

Received 00th January 20xx,
Accepted 00th January 20xx

DOI: 10.1039/x0xx00000x

www.rsc.org/

Inés R. Salcedo,[a] Rosario M. P. Colodrero,[b] Montse Bazaga-García,[a] Antonia Vasileiou,[c] Maria Papadaki,[c] Pascual Olivera-Pastor,[a] Antonia Infantes-Molina,[a] Enrique R. Losilla,[a] Gellert Mezei,[d]* Aurelio Cabeza,[a]* and Konstantinos D. Demadis[c]*

A family of alkali metal-based frameworks containing the tetraphosphonate ligand hexamethylenediamine-N,N,N′,N′-*tetrakis*(methylenephosphonic acid), HDTMP, is reported. A cation size-induced structural diversity, from monodimensional solids (Li^+ and Na^+) through layered (K^+) to pillared-layered (Rb^+ and Cs^+), was found. The proton conductivity properties for the Li compounds (hydrated and dehydrated) are reported and the influence of the dehydration/rehydration processes in enhancing proton transfer processes is highlighted. Reversible changes in the dimensionality occurred upon full dehydration/rehydration with minor rearrangements in the framework, implying variations in Li^+-ligand connectivity but preserving the tetracoordination of the metal ion. The reversibly dehydrated-rehydrated sample displayed the highest proton conductivity ($5x10^{-3}$ Scm^{-1} at 80 °C and 95 % RH), a behavior attributed to reversible formation/reformation of the P-O(H)-Li bonds that, in turn, provokes changes in the acidity of acid groups and water mobility in the temperature range of impedance measurements.

1 Introduction

The field of metal phosphonate compounds is experiencing a constant growth during the last decades.[1] This is primarily due to the rich structural diversity of these hybrids and their potential applications,[2] including gas storage,[3-5] photoluminescence,[6,7] proton conductivity,[8-14] corrosion control[15-20] and metal ion absorption.[21-22] Phosphonic acids and their water-soluble salts find extensive use in several industrial and pharmaceutical applications, such as mineral scale inhibition,[23-25] dispersion,[26] scale dissolution,[27] osteoporosis treatment,[28-30] cancer treatment,[31] etc.

Among the plethora of phosphonic acid linkers/ligands, those possessing the amino-bis(methylenephosphonate) moiety are useful tools in crystal engineering and materials synthesis because they offer the possibility of structural systematics. More specifically, a whole family of tetraphosphonate linkers can be synthetically accessed *via* the Mannich-type (Irani-Moedritzer) reaction.[32-34] In principle, this reaction allows the clean transformation of a primary amine to an amino-bis(methylenephosphonic acid) moiety. Hence, an aliphatic primary amine yields a diphosphonic acid.[35] By using α,ω-diaminoalkanes the corresponding tetraphosphonic acids can be synthesized, as shown in Scheme 1. These tetraphosphonic acids are versatile building blocks that generate a variety of structures with different topologies, including closely packed three-dimensional[36-39] and pillared layered networks[40] and some hybrids with layered structures having the phosphonic groups situated within the layers.[41,42]

[a] *Departamento de Química Inorgánica, Universidad de Málaga, Campus Teatinos s/n, Málaga-29071, Spain. E-mail: aurelio@uma.es*
[b] *Faculty of Science & Engineering, University of Wolverhampton, Wulfruna Street, Wolverhampton WV1 1LY, UK.*
[c] *Crystal Engineering, Growth and Design Laboratory, Department of Chemistry, University of Crete, Voutes Campus, Crete, GR-71003, Greece. E-mail: demadis@uoc.gr*
[d] *Department of Chemistry, Western Michigan University, Kalamazoo, Michigan 49008-5413, U.S.A. E-mail: gellert.mezei@wmich.edu*

† Electronic Supplementary Information (ESI) available: CIF files for all M-HDTMP compounds (M = Li, Na, K, Rb, Cs)], Rietveld plot for Li-HDTMP-0W, powder XRD patterns, ATR-IR spectra, additional TGA traces, graphs relating coordination number and M-O bond distances with cation size, impedance results. See DOI:10.1039/x0xx00000x

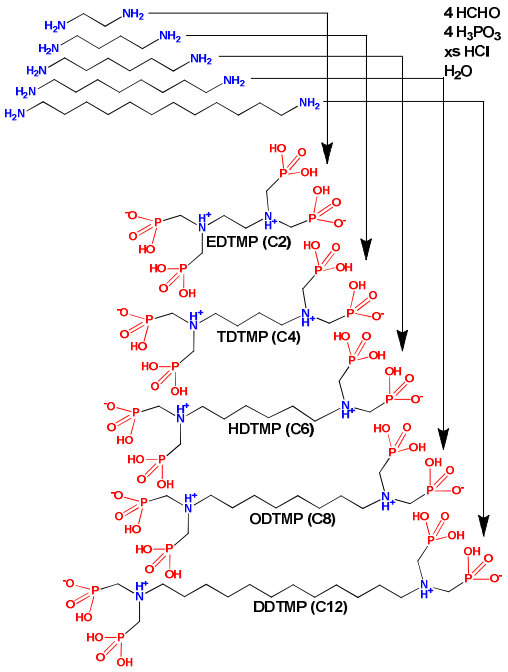

Scheme 1. Schematic structures of the tetraphosphonate family members in their zwitterionic form.

Regarding the linker HDTMP, a variety of structures ranging from 1D to 3D architectures have been reported.[40,43-48] Some representative examples of these materials are: CaHDTMP, which provided the first example of a breathing-like mechanism in metal phosphonates that presents a 2D topology,[42] La(HDTMP)·7H_2O, a 3D pillared open-framework ultramicroporous material with high proton conductivity and a strong irreversible NO adsorption capacity,[45] and [$Ln_2(SO_4)_2$(HDTMP)(H_2O)$_4$]·10H_2O (Ln = Eu^{3+}, Sm^{3+} and Gd^{3+}), a family of isotypical 3D MOFs obtained by a fast microwave-assisted methodology, which decreases considerably the reaction times for the synthesis.[49] Recently, the synthesis routes, structural diversity and properties (e.g., photoluminescence, proton conductivity, ion-exchange and heterogeneous catalysis) exhibited by lanthanide tetraphosphonic-based Metal–Organic Frameworks have been reviewed.[50]

In this paper, we report the synthesis and structural characterization of a family of alkali metal frameworks containing the ligand hexamethylenediamine-N,N,N',N'-*tetrakis*(methylenephosphonic acid), HDTMP. The proton conductivity properties for the lithium compounds are reported and the influence of the dehydration/rehydration processes in enhancing the proton transfer processes is highlighted.

2 Experimental section

2.1 Reagents and Materials. The starting alkali metal salts and hydroxides were from commercial sources and used as received (LiOH·H_2O, KOH, CsCl were from Riedel-de Haen, NaOH and RbOH from Sigma Aldrich). H_8DTMP (Dequest 2051) was from ThermPhos-Dequest, Belgium. Deionized (DI) water from a laboratory cation exchange column was used for all syntheses.

2.2 Synthesis of Alkali Metal-HDTMP Compounds. All M-HDTMP compounds were prepared in a similar manner. As an example, we provide synthetic details for **Li-HDTMP**. A general observation is that all M-HDTMP products are water-soluble and do not crystallize out from pure aqueous solutions, as several M(II), M(III) or M(IV) phosphonates do. Hence, the use of organic co-solvents as precipitants is necessary.

Li-HDTMP-4W, [Li_2(HDTMP)(H_2O)$_4$]. Solid HDTMP (0.492 g, 1.000 mmol) is added to 20 mL of DI water under stirring. Separately, LiOH·H_2O (0.042 g, 1.000 mmol) is dissolved in 10 mL DI water. The latter solution is added to the first one drop-wise, and the stirring continues until a clear colorless final solution is obtained in a glass test tube (2 cm diameter). The magnetic stirring bar is removed and 20 mL of EtOH is carefully layered on top of the aqueous layer with a Pasteur pipette, forming a H_2O/EtOH layer. The system is covered with Parafilm and left undisturbed for 2 weeks, after which large colorless needle-like crystals form. They are isolated by filtration, washed with EtOH and air-dried. Yield ~ 50 %. Elemental analysis for $Li_2(P_4O_{12}N_2C_{10}H_{26})\cdot 4H_2O$ (MW = 576.16 g/mol). Calculated, %: C 20.85, H 5.95, N 4.86. Found, %: C 20.40, H 5.83, N 5.02.

Li-HDTMP-0W, [Li_2(HDTMP)]. Heating **Li-HDTMP-4W** at 200 °C for 2 h led to a new anhydrous crystalline phase (**Li-HDTMP-0W**), which rehydrates, slowly at ambient conditions, and quickly at 80 °C and 95 % relative humidity (RH).

Na-HDTMP, [Na_2(HDTMP)(H_2O)$_{6\text{-}8}$]. The quantities used were: solid HDTMP (0.984 g, 2.000 mmol), NaOH (0.160 g, 4.000 mmol). Yield ~ 22 %. The polycrystalline solid product differs in the hydration degree with respect to the single-crystalline sample, which contains 6 water molecules per formula unit. Average elemental analysis for $Na_2(P_4O_{12}N_2C_{10}H_{26})\cdot 8H_2O$ (MW = 680.31 g/mol). Calculated, %: C 17.65, H 6.22, N 4.12. Found, %: 17.31 % C, 5.79 % H, 4.17 % N.

K-HDTMP, [K_2(HDTMP)(H_2O)$_8$]. The quantities used were: solid HDTMP (0.984 g, 2.000 mmol), KOH (0.224 g, 4.000 mmol). Yield ~ 20 %. Elemental analysis for $K_2(P_4O_{12}N_2C_{10}H_{26})\cdot 8H_2O$ (MW = 712.53 g/mol). Calculated, %: C 16.85, H 5.94, N 3.93. Found, %: C 16.76, H 5.75, N 4.01.

Rb-HDTMP, [Rb(HDTMP)(H_2O)$_2$·2H_2O]. The quantities used were: solid HDTMP (0.098 g, 0.200 mmol in 10 mL DI water), RbOH (0.04 g, 0.400 mmol in 5 mL DI water), EtOH precipitant 30 mL. Yield ~ 5 %. Polycrystalline samples are biphasic with two different hydration degrees, one of the phases corresponding to that of the single crystal sample. Average elemental analysis for $Rb(P_4O_{12}N_2C_{10}H_{27})\cdot 6H_2O$ (MW = 684.78 g/mol). Calculated, %: C 17.54, H 5.74, N 4.09. Found, %: C 17.08, H 5.01, N 4.10.

Cs-HDTMP, [Cs(HDTMP)(H_2O)$_2$·2H_2O]. *Synthesis A.* This method was followed to obtain good quality single crystals. Solid HDTMP (0.164 g, 0.300 mmol) was sonicated in 20 mL DI

water. Then a solution of CsCl (0.112 g, 0.600 mmol of CsCl in 5 mL DI water) was added to it under stirring until a clear colorless solution was obtained. A small quantity of the resulting solution (2.5 mL) was transferred to a small (0.5 cm diameter) test tube and a volume of 35 mL EtOH was carefully layered on top of the aqueous phase with a Pasteur pipette, forming a double H_2O/EtOH layer. The system was covered with Parafilm and left undisturbed for 2 weeks, after which large colorless needle-like crystals were formed. They were isolated by filtration, washed with EtOH and air-dried. Yield ~ 3 %.

Synthesis B. This method was the same as the synthesis of all other M-HDTMP compounds. The quantities used were: solid HDTMP (0.164 g, 0.300 mmol in 20 mL DI water), CsCl (0.112 g, 0.6 mmol in 5 mL DI water), EtOH precipitant 30 mL. Yield ~ 50 %. Elemental analysis for $Cs(P_4O_{12}N_2C_{10}H_{27})\cdot 4H_2O$ (MW = 696.19 g/mol). Calculated, %: C 17.25, H 5.07, N 4.02. Found, %: C 17.13, H 4.89, N 4.10.

2.3 Instrumentation. Elemental analyses (C, H, N) were measured on a Perkin–Elmer 2400 analyzer. Thermogravimetric analysis (TGA) data were recorded on an SDT-Q600 analyzer from TA instruments. The temperature varied from RT to 900 °C at a heating rate of 10 °C·min^{-1}. Measurements were carried out on samples in open platinum crucibles under air flow. Vibrational spectra were obtained with an ATR accessory coupled to FTIR spectrometer (Perkin-Elmer FT 1760). All spectra were recorded in the 4000 to 500 cm^{-1} range at 4 cm^{-1} resolution and 32 scans were accumulated.

Structural determinations. X-ray diffraction data were collected at room temperature from a single-crystal mounted atop a glass fiber under Paratone-N oil, with a Bruker SMART APEX II diffractometer using graphite-monochromated Mo-Kα (λ= 0.71073 Å) radiation. The structures were solved by employing SHELXTL direct methods and refined by full-matrix least squares on F2, using the APEX2 software package.[51] All non-H atoms were refined with independent anisotropic displacement parameters. Hydrogen atoms were placed at calculated positions and refined using a riding model, except for the water and phosphonic acid O–H hydrogens, which were located from the Fourier difference density maps and refined using a riding model with O–H distance restraints. Crystallographic details and CCDC reference codes of the crystal structures are summarized in Table 1.

Laboratory X-ray powder diffraction patterns and thermodiffraction data were collected on a PANanalytical X'Pert Pro automated diffractometer in Bragg-Brentano reflection configuration by using a Ge(111) primary monochromator (Cu $K_{\alpha 1}$) and a X'Celerator detector. Thermodiffractometric data for M-HDTMP were obtained for the samples loaded in an Anton Paar TTK450 Camera under static air. Data were collected at different temperature intervals, from room temperature up to 250 °C, for **Li-HDTMP-4W**, and at 150 °C for the other M-HDTMP derivatives. A heating rate of 5 °C·min^{-1} and a delay time of 5 minutes to ensure thermal stabilization were used. The data acquisition range was 4-70° (2θ), with a step size of 0.017° and an equivalent counting time of 230 s per step. Crystallite sizes were calculated using Williamson-Hall plot using HighScore Plus v4.6a software [PANalytical B.V.] and LaB_6 as standard for the determination of the instrumental resolution function.

Synchrotron X-ray powder diffraction data for **Li-HDTMP-0W** was collected with a beam energy of 65.341 keV [λ=0.18972(1) Å] at the ID15A beamline at the ESRF, Grenoble (France). The beam was monochromated with a double bent Laue monochromator giving a band pass of ca. 4×10^{-3} ΔE/E. Diffraction patterns were collected in transmission geometry using a Pilatus3 X CdTe 2M hybrid photon counting detector with pixel size 172×172 μm^2. The detector distance, calibrated with a pattern of CeO_2, was determined to be 1000 mm. The intensity profile was corrected for the background contribution, polarization of the X-rays and detector geometry, response, and transparency. Five images were collected with acquisition time of 8 s per image, over the angular range 0.95 - 13.50° (2θ). The glass capillary, 0.7 mm of diameter, was rotated during data collection to improve diffracting particle statistics. The powder pattern was autoindexed using the program DICVOL[52] in a triclinic cell with parameters quite similar to the as-synthesized sample. The crystal structure of **Li-HDTMP-0W** was solved by Rietveld refinement[53] using as starting model the crystal structure of **Li-HDTMP-4W**, available from single crystal determination. The refinement was carried out by using the GSAS package[54] with soft constraints to maintain chemically reasonable geometries for the phosphonate, amine groups and alkyl chains: /PO_3C tetrahedron/ P-O (1.53(1) Å), P-C (1.80(1) Å), O···O (2.55(2) Å), O···C (2.73(2) Å), /N-$(CH_2)_3$ amine group/ N-C (1.50(1) Å), C···C (2.45(2) Å) and /alkyl chain/ C-C (1.50(1) Å), $C_{chain}\cdots C_{chain}$ (2.50(2) Å. The final weight factor for the soft constrains was 15 and two isotropic atomic displacement parameter were refined, one for P atoms and a second for N, C and O atoms. For the Li atom an isotropic displacement paramenter was fixed (0.04 Å^2). The final Rietveld plot is given in Figure S1 (Electronic Supplementary Information) and the most relevant crystallographic data are presented in Table 1.

Proton conductivity studies. Impedance data were collected on ~ 1 mm thickness cylindrical pellets (~ 5 mm in diameter), which were obtained by pressing ~ 40 mg of sample at 250 MPa for 2 min between porous C electrodes (Sigracet, GDL 10 BB, no Pt). The sample cell was placed inside a temperature and humidity controlled chamber ESPEC SH-222 and connected to an AUTOLAB PGSTAT302N analyzer over the frequency range from 20 Hz to 10^5 Hz with an applied voltage of 0.35 V. To equilibrate water content, pellet was first preheated (0.2 °C/min) from 25 to 80 °C and 95 % of relative humidity (RH). Impedance spectra were recorded on cooling using a stabilization time of 5 h at 20 °C intervals and variable relative humidity values (60 % and 95 % RH). Water condensation on sample was avoided by reducing first the relative humidity before decreasing temperature. All measurements were electronically controlled by the winDETA package of programs.[55]

Journal Name

ARTICLE

Table 1. Selected crystallographic data for the **M-HDTMP** (M = Li, Na, K, Rb and Cs) compounds.

Phase	Li-HDTMP-4W	Li-HDTMP-0W	Na-HDTMP	K-HDTMP	Rb-HDTMP	Cs-HDTMP
Space group	$P\bar{1}$	$P\bar{1}$	$P\bar{1}$	$P2_1/c$	C2/c	$P\bar{1}$
Chemical formula	$Li_2P_4O_{16}N_2C_{10}H_{34}$	$Li_2P_4O_{12}N_2C_{10}H_{26}$	$Na_2P_4O_{23}N_2C_{10}H_{48}$	$K_2P_4O_{20}N_2C_{10}H_{42}$	$RbP_4O_{16}N_2C_{10}H_{35}$	$CsP_4O_{16}N_2C_{10}H_{35}$
Formula Mass (g/mol)	576.16	504.10	734.36	712.53	648.75	696.19
λ (Å)	0.71073	0.18972	0.71073	0.71073	0.71073	0.71073
a (Å)	5.9728(6)	5.9014(4)	7.66820(10)	7.71780(10)	6.0257(5)	6.0072 (2)
b (Å)	9.4557(9)	9.2693(7)	11.53350(10)	33.0373(4)	14.1011(7)	7.6864(2)
c (Å)	11.0182(11)	9.5123(7	18.0768(2)	11.75770(10)	28.762(2)	14.8250(4)
α (°)	74.418(7)	85.902(4	97.3780(10)	90.00	90.00	86.677(2)
β (°)	76.170(7)	77.676(5)	94.7920(10)	103.7090(10)	94.816(3)	78.906(2)
γ (°)	84.313(7)	85.588(6)	101.7050(10)	90.00	90.00	67.611(2)
V ($Å^3$)	581.622(10)	506.04(8)	1542.61(3)	2912.52(6)	2435.25(6)	621.01(3)
Crystal size (mm)	0.22×0.05×0.04	-	0.45×0.22×0.03	0.50×0.20×0.05	0.50×0.21×0.09	0.10×0.07×0.03
Z	1	1	2	4	4	1
ρ_{calc} ($g.cm^{-3}$)	1.645	1.568	1.526	1.782	1.721	1.862
2θ range (°)	2.58-24.54	0.187-13.501	1.82-31.03	1.89-30.02	1.41-33.45	2.87-27.91
Data/Restrains/ Parameters	1719/7/175	1428/94/33	7729/28/457	7448/22/409	3984/10/189	2722/8/176
Nº reflections	10054	2254	9784	8877	4773	3748
Independent reflections [I > 2σ(I)]	1693	-	7729	7448	3984	2722
R_{wp}	-	0.0115	-	-	-	-
R_p	-	0.0220	-	-	-	-
R_F	-	0.0427	-	-	-	-
GoF	0.991	-	1.052	1.036	1.039	1.024
R Factor [I > 2σ(I)]	[a]R1 = 0.0578, [a]wR2 = 0.1399	-	[a]R1 = 0.0368, [a]wR2 = 0.0905	[a]R1 = 0.0287, [a]wR2 = 0.0666	[a]R1 = 0.0328, [a]wR2 = 0.0791	[a]R1 = 0.0344, [a]wR2 = 0.0676
R Factor (all data)	[a]R1 = 0.0904, [a]wR2 = 0.1595	-	[a]R1 = 0.0527, [a]wR2 = 0.0981	[a]R1 = 0.0393, [a]wR2 = 0.0713	[a]R1 = 0.0436, [a]wR2 = 0.0838	[a]R1 = 0.0580, [a]wR2 = 0.0759
CCDC Code	1584820	1584815	1584819	1584817	1584816	1584818

Solid-State NMR. ^{1}H MAS (magic angle spinning) NMR spectra were performed in a Bruker Ascend-600 spectrometer equipped with a 2.5 mm MAS probe with an operating frequency for protons of 600.09 MHz. ^{1}H spectra were at a spinning rate of 30 kHz, with a pulse of width of 2 micros, dwell time 6.50 µs and 3 s of delay. ^{1}H chemical shifts were

indirectly referenced by using adamantane as an external reference. The deconvolution of ^{1}H MAS-NMR spectra were carried out using the DMFIT program to obtain the different components and their contributions.[56]

3 Results and discussion

In general, polycrystalline samples display higher water content than the corresponding single crystals. This excess of water is related to the presence of other more hydrated polycrystalline phases (*eg.* **Na-** and **Rb-HDTMP**) coexistent with those corresponding to the single crystal phases, as can be inferred from a comparison between the simulated from single crystal and the polycrystalline samples XRD patterns (Figure S2-upper). However, water content in **Li-, K-** and **Cs-HDTMP** derivatives is in good agreement with that of the corresponding to the single crystals (Figure S2).

All new compounds were characterized by ATR-IR spectroscopy (Figure S2-lower), which allowed differentiation of different structural modes of the phosphonate groups. Vibrations of the P-OH moiety appear in the 890-940 cm^{-1} region. Peaks around 1040 cm^{-1} and 1250 cm^{-1} are assigned to the asymmetric P=O stretch. The $-PO_3$ stretch appears as a strong band in the region 1085-1165 cm^{-1}, whereas the bending of $-PO_3$ shows up in the 400-600 cm^{-1} region. The O-H stretching vibration is noted as a multitude of broad bands in the region 3200-3600 cm^{-1}, while bending vibrations are at ~ 1640 cm^{-1}, all originating from bound or lattice water.

3.1 Crystal structures of "free" HDTMP and Li-HDTMP compounds.

HDTMP. The crystal structure of the free HDTMP acid has been reported by us elsewhere.[57] It crystallizes as the anhydrous form, and is located on an inversion center within the triclinic (Pī) crystal lattice. Two phosphonate groups (one on each side) of the zwitterionic molecule are singly deprotonated ($-PO_3H^-$), whereas the other two are fully protonated ($-PO_3H_2$). The tertiary N atoms are also protonated. This is a common phenomenon in the crystal structures of amino-bis(methylenephosphonates.[58] An extended 3D-network is formed by H-bonding between the phosphonate groups and NH^+ moieties (Figure S3, Table S1 in the SI).

Li-HDTMP compounds. The crystal structure of **Li-HDTM-4W**, solved by single-crystal X-ray diffraction, contains an inversion center within the triclinic (Pī) crystal lattice (Figure 1). The HDTMP ligand has all phosphonate moieties singly deprotonated ($-PO_3H^-$). Both N atoms are protonated; hence, the entire HDTMP molecule is dianionic. Lithium is tetrahedrally coordinated by four oxygen atoms, originating from two water molecules and two phosphonate oxygens from two different HDTMP molecules, thus creating rings built up of two ligand molecules and two metal ions. The rings are stabilized by H-bonds between phosphonate groups and extend into 1D-ribbons (Figure 2a). These ribbons are connected by further H-bonds to the NH^+ moieties and H_2O molecules (Figure 2b, and Table S1).

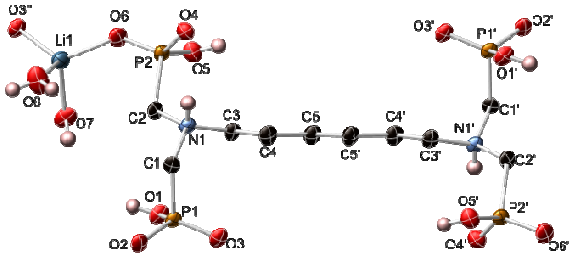

Fig. 1 Thermal ellipsoid plot (50% probability) of **Li-HDTMP**, showing the tetrahedral coordination sphere around the Li^+ ion (C–H hydrogens not shown for clarity). Symmetry operators: (') x+1/2, –y, –z+1; ('') x, y+1, z.

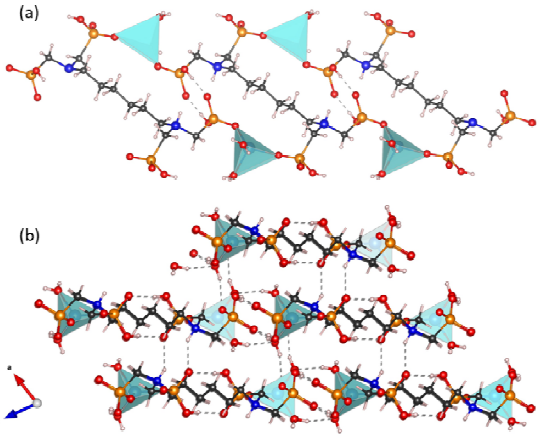

Fig. 2 View of the **Li-HDTMP-4W** structure showing (a) the 1D-ribbon motifs and (b) packing of the 1D-ribbon with H-bond interactions (2.7 <D-H···A<2.99 Å) marked.‡

The thermodiffractometric study (Figure 3) revealed that the solid Li-HDTM-4W maintains its stability up to ~ 120 °C. By further heating, a second phase clearly develops from 140 °C and remains as the unique crystalline phase up to 220 °C.

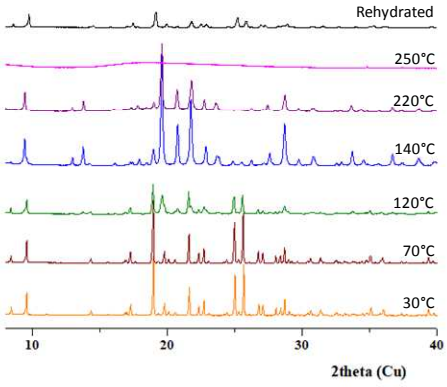

Fig. 3 Thermodiffraction patterns for the **Li-HDTMP-4W** compound.

As demonstrated below, this new phase is anhydrous (Li-HDTM-0W). The water is lost in a stepwise fashion between 100 °C and 220 °C (calculated, 15.2 %; found, 15.1 %). An additional weight loss, observed in the range 220 – 300 °C, is attributed to partial condensation of P-OH groups as compared with the thermal behaviour of the free phosphonic acid (Figure 4). This process induces amorphization before decomposition, which takes place at ~300 °C. Importantly, **Li-HDTM-0W** is reversibly hydrated to the initial phase by long exposure at ambient conditions or short exposure (5 h) at 80 °C and 95 % RH.

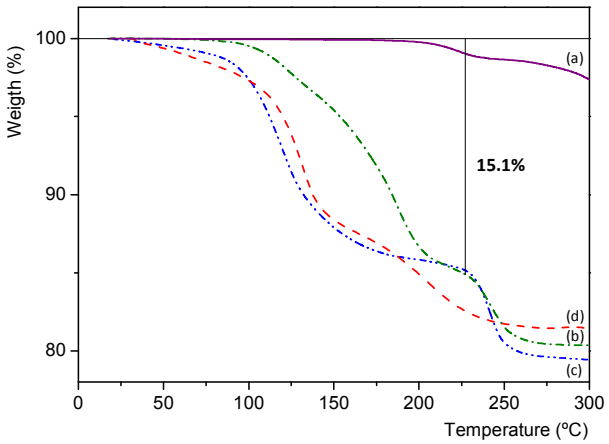

Fig. 4 Thermal analysis for compounds, (a) HDTMP; (b) **LiHDTMP-4W**, (c) **Li-HDTMP** after impedance measurements, and (d) rehydrated **Li-HDTMP-0W**.

The crystal structure of Li-HDTM-0W, Figure 5, can be viewed as a result of the condensation of the ribbon-like chains into a 2D framework, in which the tetrahedral coordination of the lithium atoms is preserved by increasing the connectivity of the phosphonate groups with respect to the metal ions. In this new structure, 16-membered rings are created through formation of edge-sharing LiO_6 dimers extended along the *a*-axis.

3.2 Crystal structure of M-HDTMP (M = Na^+, K^+, Rb^+ and Cs^+).

Na-HDTMP crystallizes in the triclinic ($P\bar{1}$) crystal system, with the ligand moiety being located on a general position and having all phosphonate groups singly deprotonated ($-PO_3H^-$) (Figure 6). Both N atoms are protonated, hence the entire HDTMP molecule is dianionic. There are three crystallographically independent Na^+ ions in the lattice. Two of these (Na1 and Na3) are located on inversion centers. Na1 and Na2 are 6-coordinated, the former by two phosphonate O-atoms (from two different ligand molecules) and four water O-atoms, and the latter by one phosphonate O-atom and four water O-atoms. Na1 and Na2 are bridged by H_2O molecules and coordinate to HDTMP moieties to form a 1D-ribbon (Figure 6) of edge- and face-sharing octahedra. Na3 serves as counter ion in the form of octahedral $[Na(H_2O)_6]^+$. The 1D-ribbons are connected to each other and the $[Na(H_2O)_6]^+$ counterions by H-bonding via multiple lattice H_2O molecules (Figure 6).

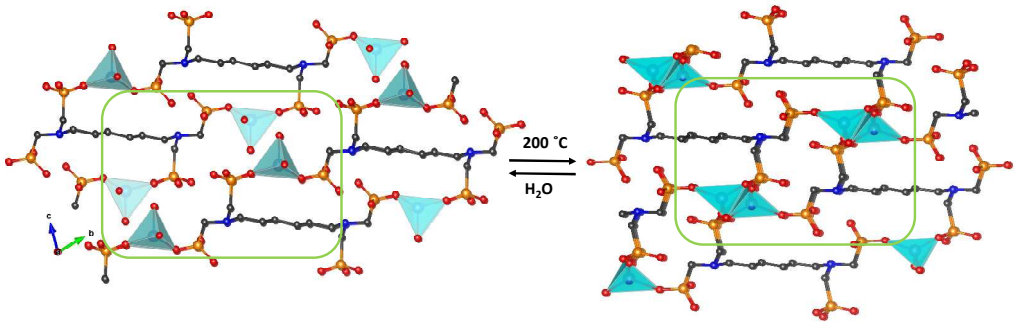

Fig. 5 Reversible structural transformation of **Li-HDTMP** compounds upon carrying out dehydration-rehydration cycles.

Journal Name

ARTICLE

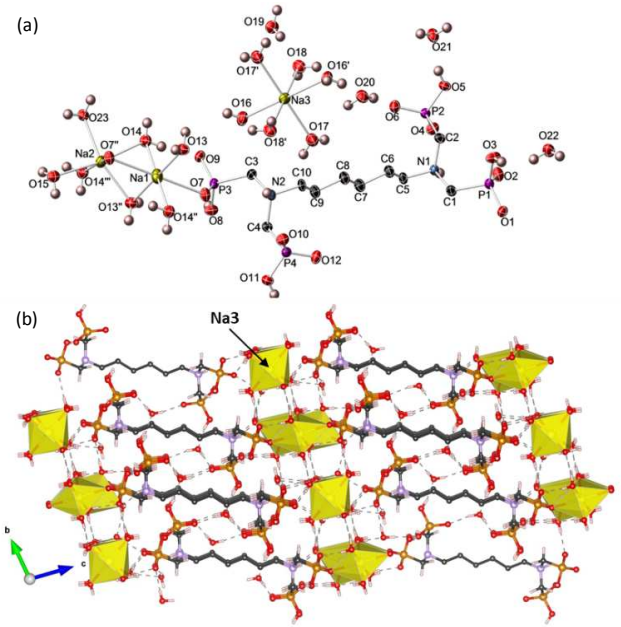

Fig. 6 (a) Thermal ellipsoid plot (80% probability) of Na-HDTMP showing the coordination sphere around the Na^+ ions. Symmetry operators: (') –x+2, –y+1, –z+2; ('') –x, –y, –z+2; (''') –x–1, –y, –z+2. (b) 3D-packing of the 1D-ribbons in Na-HDTMP (C–H hydrogens not shown for clarity). (b) 3D-packing of the 1D-ribbons in Na-HDTMP (C–H hydrogens are omitted for clarity).

K-HDTMP exhibits a monoclinic lattice ($P2_1/c$) where the ligand is also dianionic as in the case of Na-HDTMP (Figure 7a). There are two crystallographically independent K^+ ions in the lattice: K1 is heptacoordinate by three phosphonate O-atoms (from two different ligand molecules) and four water O-atoms, and K2 is hexacoordinate by one phosphonate O-atom and five water O-atoms. K1 and K2 form face-sharing dimers through three oxygens from two water molecules (O13 and O14) and one phosphonate group (O2). These dimers are connected to each other by one bridged H_2O molecule (O17) given rise to chains interconnected by the HDTMP ligand (Figure 7b). The zig-zag layers generated are packed through H-bonds, assisted by lattice waters located between them.

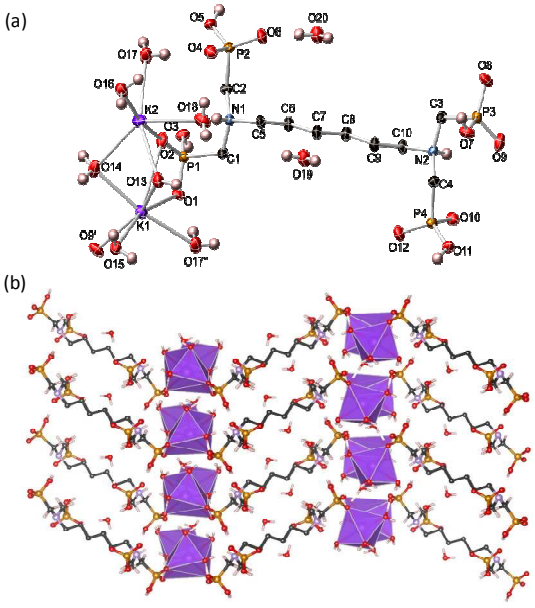

Fig. 7 (a) Thermal ellipsoid plot (80% probability) of K-HDTMP, showing the coordination sphere around the K^+ ions and connectivity of the chains. Symmetry operators: (') –x+1, y–1/2, –z+3/2; ('') x+1, y, z. (b) view of the layered structure of K-HDTMP (C–H hydrogens not shown for clarity).

In the monoclinic lattice (C2/c) of **Rb-HDTMP**, the Rb^+ ions are located on a C_2 axis and are octacoordinate by six phosphonate O-atoms (from four different ligand molecules) and two water O-atoms. As with K^+, the Rb^+ ions in **Rb-HDTMP** form sheets, which are connected to each other by dianionic HDTMP ligand molecules. In contrast to the K-salt, however, the sheet is formed by isolated phosphonate-bridged Rb^+ polyhedra (Figure 8). In this framework, the HDTMP ligand also connects sheets into a pillared layered structure with the lattice water situated inside the interlayer space giving rise to an H-bond network (Figure 8).

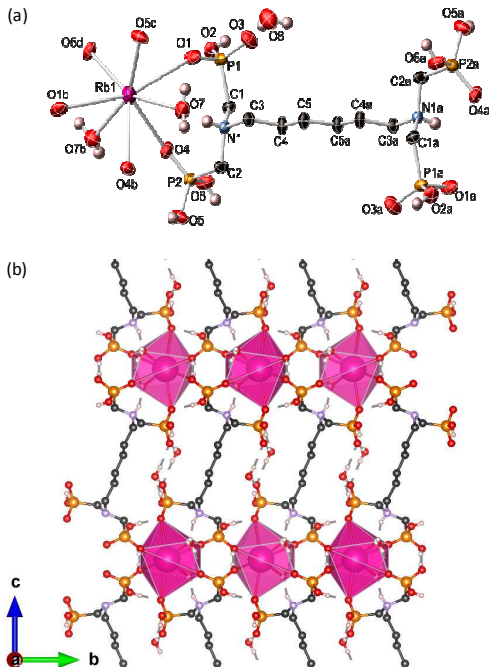

Fig. 8 (a) Thermal ellipsoid plot (50% probability) of Rb-HDTMP, showing the coordination sphere around the Rb ion (only one of the two disordered O7 atoms is shown for clarity). Symmetry operators: (a) –x+2, y–1, –z+1; (b) –x+1, y, –z+1/2; (c)–x+1/2, y–1/2, z; (d) –x+1/2, y–1/2, –z+1/2. (b) View of the pillared layered structure of Rb-HDTMP (C–H hydrogens not shown for clarity).

Within the triclinic (P$\bar{1}$) lattice of **Cs-HDTMP**, the Cs^+ ions are located on an inversion center and are octacoordinate by six phosphonate O-atoms (from four different ligand molecules) and two water O-atoms. Sheets are formed by edge-sharing Cs^+ polyhedra bridged by phosphonate groups (Figure 9). The sheets are similarly connected by doubly deprotonated HDTMP ligand molecules into a pillared-layered structure (Figure 9) containing H-bonded lattice water.

The thermal behaviour of compounds **M-HDTMP** (M = Na, K, Rb, Cs) follows a similar dehydration pattern before decomposition at *ca* 240 °C (Figure S4). The Na^+ salt showed the highest divergence in hydration respect to the single crystal (observed, 22.42 %; calculated 16.76%). The weight loss observed for **K-HDTMP**, 20.40%, agrees well with the calculated value for full dehydration of the compound (calculated 20.22%). **Rb-HDTMP** shows several consecutives weight losses between RT and 240 °C. The observed weight loss, 12.92%, is slightly higher than the calculated value, taking into account the composition of the single crystal analysed (11.11 %). As corroborated by thermodiffraction (Figure S5), the polycrystalline sample lost labile water below 80 °C. At this temperature, the X-ray powder diffraction pattern agrees well with one simulated from the single crystal data. Further heating leads to the amorphization of the solid. **Cs-HDTMP** starts losing water at ~ 100 °C, with a total weight loss corresponding to 4 water molecules (observed 9.57%, calculated 10.34%).

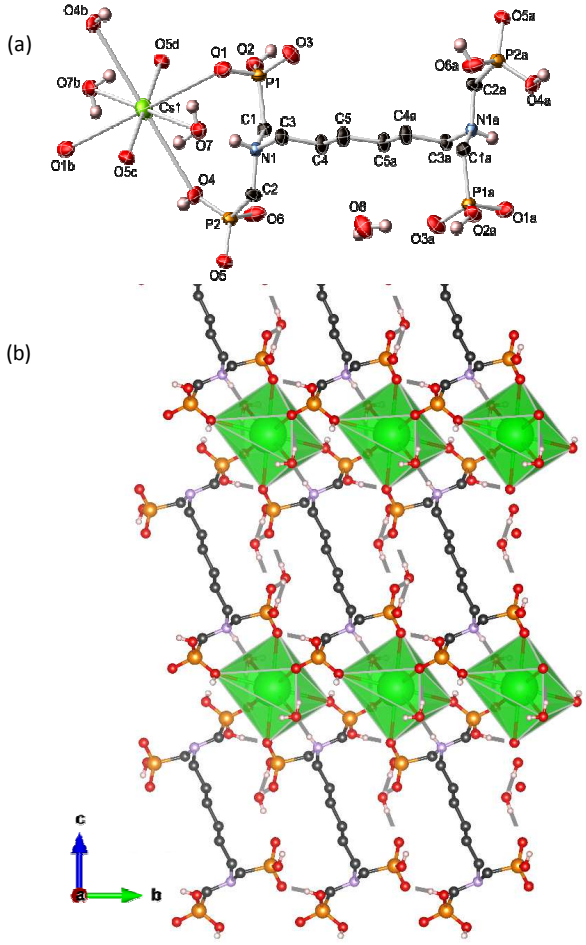

Fig. 9 (a) Thermal ellipsoid plot (50% probability) of Cs-HDTMP, showing the coordination sphere around the Cs ion. Symmetry operators: (a) –x, y–1, –z+2; (b) –x+1, –y+2, –z+1; (c)–x+1, –y+1, –z+1; (d) x, y+1, z. (b) View of the pillared layered structure of Cs-HDTMP (C–H hydrogens not shown for clarity).

Despite the observed trend of increasing ligand denticity towards larger M^+ cations, a direct relationship between the M^+ radius and the average M-O bond distance is maintained (Figure S6). The complexity of the M-HDTMP structures deserves further discussion. The effect of the alkali metal ionic radii is reflected not only on the M-O bond distances (either with water or phosphonate oxygens), but also on the coordination number of the metal center. The tetrahedral Li^+ cations in the structure of **Li-HDTMP** are 4-coordinated (by two different HDTMP ligands and two water molecules). The structure adopted is 1D "ribbon" or "slab". The Na^+ ions in the structure of **Na-HPAA** are 6-coordinated (by one phosphonate oxygen and five water molecules). The structure adopted is 1D with $Na(H_2O)_6^+$ counter ions for charge balance. The K^+ cations in the 3D structure of **K-HDTMP** are 6-coordinated (by one

phosphonate oxygen and five waters) and 8-coordinated (by three phosphonate oxygens and five waters). The Rb^+ cations in the 3D structure of **Rb-HDTMP** are 8-coordinated (by six phosphonate oxygens and two waters). Finally, the largest cation Cs^+ is 10-coordinated in the 3D structure of **Cs-HDTMP** (four HDTMP ligands, eight phosphonate oxygens and two water molecules). These observations are in line with previous reports on alkali-HPAA[59] and alkaline-earth metal HPAA[47,60-64] (HPAA = hydroxyphosphonoacetic acid) systems and/or alkaline-earth AMP[65-67] (AMP = amino-*tris*(methylenephosphonic acid) systems.

3.3 Proton conduction

The structural features exhibit by these compounds, with extended H-bonding networks, make them potential candidates as proton conductors. Preliminary stability tests performed at high RH values showed that all compounds except lithium derivative are highly hygroscopic materials. Therefore only the proton conductivity properties of **HDTMP** and **Li-HDTMP** solids were studied. Impedance spectra at different temperatures and RH for **HDTMP** and **Li-HDTMP** compounds are shown in Figures S7. The total pellet resistance, R_T, was obtained from the intercept of the spike and/or the arc (low- frequency end) on the Z' axis. Arrhenius plots, Figure 10, show the overall pellet conductivities for **HDTMP** and **Li-HDTMP** compounds between 25 and 80 °C. As can be seen, the proton conductivity of the "free" **HDTMP** phosphonic acid dramatically increases nearly three orders of magnitude with the RH from 9.2×10^{-7} S·cm^{-1} (60 %, 80 °C) to 2.2×10^{-4} S·cm^{-1} (95 %, 80 °C). It has been reported that the proton conductivity of phosphonic acids is higher for crystalline than for amorphous phases. This behavior is correlated with self-assembly of phosphonic groups generating regions with high concentration of H-bonds and, hence, providing high proton conductivity values in ordered compounds.[68] Figure S3 displays the packing of the ligand molecules where hydrogen-bond interactions are apparent along the *a*-axis. In this case, not only the phosphonic groups are involved but also the protonated amine groups contribute to the extended network. As already demonstrated,[68] the structural arrangement in crystalline phosphonic acids may facilitate the adsorption of small amount of water (< 1 % from TG for HDTMP) upon increasing the relative humidity, giving rise to extended H-bond networks that significantly enhance proton conductivity. The low activation energy (0.29 eV) determined from the Arrhenius plot (Figure 10) indicates that a Grotthuss proton transfer mechanism operates at high humidity.[69] Post-impedance powder diffraction pattern of HDTMP did not show any structural change (Figure S8)

The as synthesized **Li-HDTMP-4W** shows higher proton conductivity values ($7.6\text{x}10^{-4}$ S·cm^{-1} at 80 °C and 95 % RH) than the free HDTMP attributed to the presence of coordinated water in the structure of the former, which contributes to establish additional H-bond interactions with the acidic groups of the ligand and, hence, more extended proton transport pathways (see Table S1) are former in the lithium derivative structure. The activation energy values found for this compound (Figure 10), is 0.41 eV at 95 % RH and increases slightly up to 0.54 eV at 60 % RH, which suggests a gradual change in proton transfer from Grotthuss to vehicle mechanism. **Li-HDTMP-0W** rehydrates to **Li-HDTMP-4W** upon preheating the sample at 80 °C and 95 % RH for 5 h, therefore the conductivity measurements correspond to the fully hydrated compound (Figure S9). Interestingly, this sample displays proton conductivity values almost one order of magnitude higher that as synthesized **Li-HDTMP-4W** ($5\text{x}10^{-3}$ S·cm^{-1} versus $7.6\text{x}10^{-4}$ S·cm^{-1} at 80 °C and 95 % RH). In order to a better understanding of this behavior, Rietveld-determined particle size, solid state ^{1}H-MAS-NMR and TG analysis were performed. After impedance measurements, a half particle size reduction was determined for both samples, from ~ 1400 Å to ~ 700 Å for the as synthesized sample, and from ~ 1200 Å to ~ 600 Å for the rehydrated **Li-HDTMP-0W**; resulting pellets with similar compactions (~ 85 %).

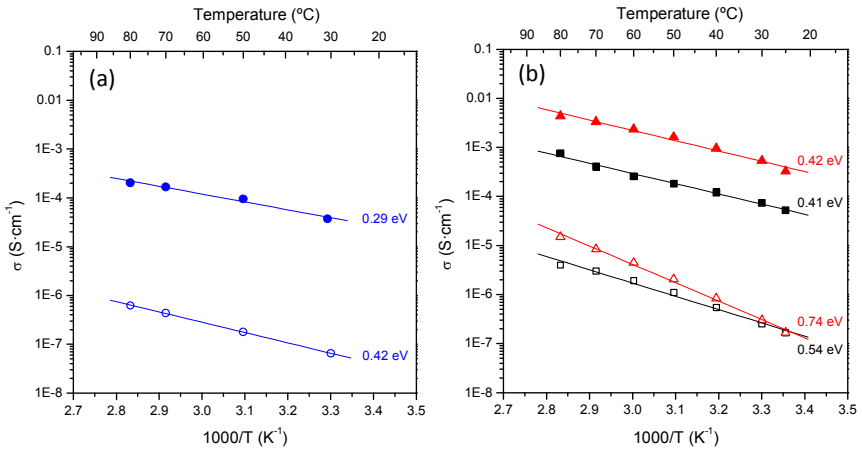

Fig. 10 Arrhenius plots for: (a) **HDTMP** acid and (b) as synthesized **Li-HDTMP-4W** (squares) and rehydrated **Li-HDTMP-0W** (triangles) at 60% RH (empty) and 95% RH (filled).

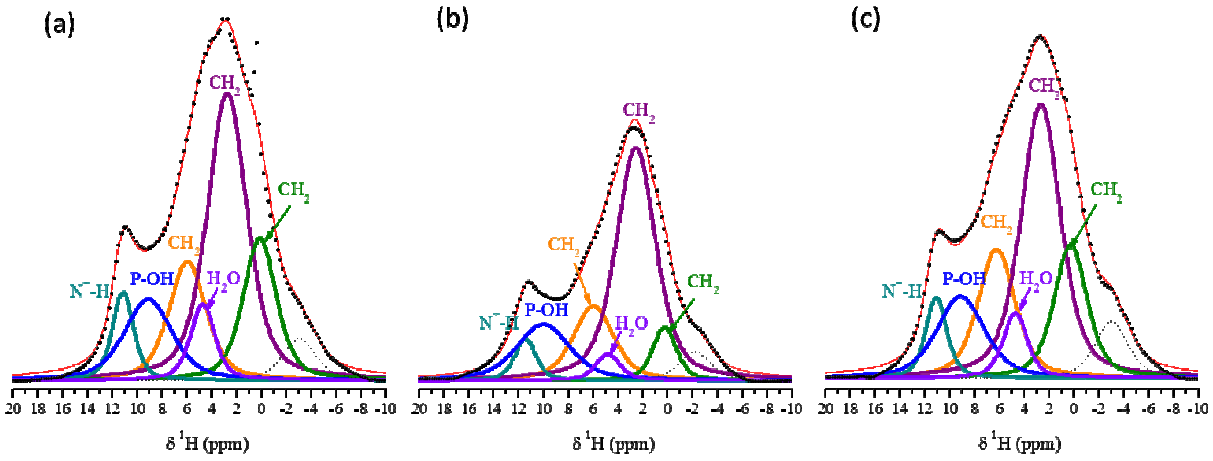

Fig. 11 Solid state ^{1}H-MAS-NMR spectra showing the fitting to several components for (a) **Li-HDTMP-4W**, (b) **Li-HDTMP-0W** and (c) rehydrated **Li-HDTMP-0W**. The bands located near −3 ppm are due to the signal probe.

^{1}H-MAS-NMR spectra for all **Li-HDTMP** compounds were collected. Figure 11 shows the spectra for **Li-HDTMP-4W as synthesized (a), Li-HDTMP-0W (b)** and rehydrated **Li-HDTMP-0W (c)**. They consist of broad bands that can be deconvoluted into several components. Together with the signals corresponding to the -CH_2- groups (Table S2), the bands appearing in the spectra at 8.6 ppm and 11.0 ppm are assigned to P-OH and N-H^+ groups, respectively,[70] whereas that at ~5.0 ppm correlates with bound water.[71] For all **Li-HDTMP** compounds, the post-impedance spectra were quite similar, confirming that they correspond to the same fully hydrated structure.

However, the TG curves (Figure 4) reveal subtle variations in the water loss, which suggest that a change in water interactions occurred in the framework. The rehydration process implies the breaking of the P-O(H)-Li bonds and its transformation P-OH + Li-OH_2 (Figure 5). It can be speculated that a memory effect is preserved in the rehydrated **Li-HDTMP-0W** sample that makes easier the reformation of the P-O(H)-Li bonds and, hence, leading to changes in the acidity of acid groups and water mobility what would justify the changes in the conductivity.

Conclusions

Reactions of the flexible tetraphosphonate ligand **HDTMP** with the alkali metal ion series generate a cation size-induced structural diversity from monodimensional solids (Li^+ and Na^+) through layered (K^+) to pillared-layered (Rb^+ and Cs^+) structures with water exhibiting a pleiotropic role: (a) as metal-bound terminal ligand, (b) as bridging ligand, and (c) as H-bonding donor and acceptor. These multiple roles give rise to different proton transport pathways. While the Na^+- to Cs^+-salts are highly hygroscopic materials, the lithium derivative shows a high thermal stability and reversible dehydration/rehydration between 25 °C and 200 °C. Through this process, the proton conductivity is enhanced almost one order of magnitude, reaching the value of $5x10^{-3}$ Scm^{-1} (80 °C and 95 % RH). This effect is attributed to subtle changes in the interaction of water molecules and acidity within the crystalline structure.

Conflicts of interest

There are no conflicts to declare.

Acknowledgements

The work at UoC was supported by grants from the Research Committee of the University of Crete, ELKE, (Grant # KA 3806). The work at UMA was funded by MAT2016-77648-R research grant (Spain) which is co-funded by FEDER and by Junta de Andalucía (Spain) P12-FQM-1656. A.I.M. thanks the Ministry of Economy and Competitiveness for a Ramon y Cajal contract (RyC2015-17870). The work at WMU was supported by the US National Science Foundation under Grant No. CHE-1404730.

Notes and references

‡K. Momma and F. Izumi, "VESTA 3 for three-dimensional visualization of crystal, volumetric and morphology data," *J. Appl. Crystallogr.*, 2011, **44**, 1272-1276.

1 A. Clearfield, K.D. Demadis, (Eds.) *Metal Phosphonate Chemistry: From Synthesis to Applications*, Royal Society of Chemistry, Cambridge, U.K., 2012.

2 E. Brunet, J.L. Colón, A. Clearfield (Eds.) Tailored Organic-Inorganic Materials, John Wiley & Sons, Inc., New York, U.S.A. 2015.
3 M.T. Wharmby, J.P.S. Mowat, S.P. Thompson, P.A. Wright, *J. Am. Chem. Soc.,* 2011, **133**, 1266–1269.
4 S.R. Miller, G.M. Pearce, P.A. Wright, F. Bonino, S. Chavan, S. Bordiga, I. Margiolaki, N. Guillou, G. Ferey, S. Bourrelly, P.L. Llewellyn, *J. Am. Chem. Soc.,* 2008, **130**, 15967–15981.
5 K. Maeda, *Microporous Mesoporous Mater.,* 2004, 73, 47–55.
6 R.F. Mendes, D. Ananias, L.D. Carlos, J. Rocha, F.A. Almeida Paz, *Cryst. Growth Des*., 2017, **17**, 5191-5199.
7 G.-T. Wang, Z.-Y. Tang, H.-T. Zhou, P. Zou, *Polyhedron*, 2016, **117**, 259-264.
8 A. Donnadio, M. Nocchetti, F. Costantino, M. Taddei, M. Casciola, F. da Silva Lisboa, R. Vivani, *Inorg. Chem.*, 2014, **53**, 13220-13226.
9 S. Begum, Z. Wang, A. Donnadio, F. Costantino, M. Casciola, R. Valiullin, C. Chmelik, M. Bertmer, J. Kärger, J. Haase, H. Krautscheid, *Chem. Eur. J.*, 2014, **20**, 8862-8866.
10 S.-S. Bao, G.K.H. Shimizu, L.-M. Zheng, *Coord. Chem. Rev.,* 2017, in press, DOI: 10.1016/j.ccr.2017.11.029.
11 S.-S. Bao, N.-Z. Li, J.M. Taylor, Y. Shen, H. Kitagawa, L.-M. Zheng, *Chem. Mater.,* 2015, **27**, 8116−8125.
12 J.M. Taylor, R.K. Mah, I.L. Moudrakovski, C.I. Ratcliffe, R. Vaidhyanathan, G.K.H. Shimizu, *J. Am. Chem. Soc.,* 2010, **132**, 14055–14057.
13 Z.H. Fard, N.E. Wong, C.D. Malliakas, P. Ramaswamy, J.M. Taylor, K. Otsubo, G.K.H. Shimizu, *Chem. Mater.,* 2018, **30**, 314−318.
14 J. Zhang, L. Chen, D. Gui, H. Zhang, D. Zhang, W. Liu, G. Huang, J. Diwu, Z. Chai, S. Wang, *Dalton Trans.,* 2018, **47**, 5161-5165.
15 K.D. Demadis, C. Mantzaridis, P. Lykoudis, *Ind. Eng. Chem. Res.,* 2006, **45**, 7795-7800.
16 M. Papadaki, K.D. Demadis, *Comments Inorg. Chem.,* 2009, **30**, 89-118.
17 R.M.P. Colodrero, G.K. Angeli, M. Bazaga-Garcia, P. Olivera-Pastor, D. Villemin, D.; E.R. Losilla, E.Q. Martos, G.B. Hix, M.A.G. Aranda, K.D. Demadis, A. Cabeza, *Inorg. Chem.,* 2013, **52**, 8770–8783.
18 S.A. Umoren, M.M. Solomon, *J. Environ. Chem. Engin.,* 2017, **5**, 246–273
19 D.-M. Zang, D.-K. Cao, L.-M. Zheng, *Inorg. Chem. Commun.,* 2011, **14**, 1920–1923.
20 A. Mesbah, S. Jacques, E. Rocca, M. François, J. Steinmetz, *Eur. J. Inorg. Chem.,* 2011, 1315–1321.
21 A. Popa, C.-M. Davidescu, N. Petru, I. Gheorghe, A. Katsaros, K.D. Demadis, *Ind. Eng. Chem. Res.,* 2008, **47**, 2010-2017.
22 A.-L. Alanne, M. Tuikka, K. Tnsuaadu, M. Ylisirniö, L. Hämäläinen, P. Turhanen, J. Vepsäläinen, S. Peräniemi, *RSC Adv.,* 2013, **3**, 14132-14138.
23 E. Barouda, K.D. Demadis, S. Freeman, F. Jones, M.I. Ogden, *Cryst. Growth Des.,* 2007, **7**, 321-327.
24 Z. Amjad, A. Kweik, *Phosphorus Res. Bull.,* 2015, **30**, 19-25.
25 Z. Amjad, R.T. Landgraf, J.L. Penn, *Int. J. Corros. Scale Inhib.,* 2014, **3**, 35–47.
26 Q. Luo, *Ind. Eng. Chem. Res.,* 2000, **39**, 3249-3254.
27 K.D. Demadis, E. Mavredaki, M. Somara, M. *Ind. Eng. Chem. Res.,* 2011, **50**, 13866–13876.
28 K.E. Papathanasiou, P. Turhanen, S.I. Brückner, E. Brunner, K.D. Demadis, *Sci. Rep.,* 2017, **7**, Article number 4743.
29 R.W. Sparidans, I.M. Twiss, S. Talbot, *Pharm. World Sci.,* 1998, **20**, 206-213.
30 F. Cheng, Eric Oldfield, *J. Med. Chem.,* 2004, **47**, 5149-5158.
31 G. De Rosa, G. Misso, G. Salzano, M. Caraglia, *J. Drug Delivery,* 2013, Article ID 637976.
32 K. Moedritzer, R.R. Irani, *J. Org. Chem.,* 1966, **31**, 1603–1607.
33 P.B. Iveson, M.P.L. Lowe, J.C. Lockhart, *Polyhedron,* 1993, **12**, 2313-2323.
34 E.D. Naydenova, P.T. Todorov, K.D. Troev, *Amino Acids,* 2010, **38**, 23–30.
35 D. Villemin, M.A. Didi, *Orient. J. Chem.,* 2015, **31**, 1-12.
36 N. Stock, T. Bein, *Angew. Chem. Int. Ed.*, 2004, **43**, 749 –752.
37 N. Stock, A. Stoll, T. Bein, *Microporous Mesoporous Mater.,* 2004, **69**, 65-69.
38 N. Stock, N. Guillou, J. Senker, G. Férey, T. Bein, *Z. Anorg. Allg. Chem.*, 2005, **631**, 575–581.
39 N. Stock, M. Rauscher, T. Bein, *J. Solid State Chem.,* 2004, **117**, 642-647.
40 F. Costantino, T. Bataille, N. Audebrand, E., Le Fur, C. Sangregorio, *Cryst. Growth Des.,* 2007 , *7*, 1881-1888.
41 R. Vivani, F. Costantino, U. Costantino, M. Nocchetti, *Inorg. Chem.*, 2006, **45**, 2388-2390.
42 R.M.P. Colodrero, A. Cabeza, P. Olivera-Pastor, A. Infantes-Molina, E. Barouda, K.D. Demadis, M.A.G. Aranda, *Chem. Eur. J.*, 2009, **15**, 6612–6618.
43 K.D. Demadis, E.,Barouda, R.G. Raptis, H. Zhao, *Inorg.Chem.*, 2009, **48**, 819-821.
44 G.-L. Zheng, J.-F. Ma, J. Yang, *J. Chem. Res.*, 2004, 387–388.
45 R.M.P. Colodrero, P. Olivera-Pastor, E.R. Losilla, M.A.G. Aranda, L. León-Reina, M. Papadaki, A.C. McKinlay, R.E. Morris, K.D. Demadis, A. Cabeza, *Dalton Trans.*, **2012**, 41, 4045-4051.
46 K.D. Demadis, C. Mantzaridis, R.G. Raptis, G. Mezei, *Inorg. Chem.*, 2005, **44**, 4469-4471.
47 K.D. Demadis, N. Stavgianoudaki, in *Metal Phosphonate Chemistry: From Synthesis to Applications*, A. Clearfield, K.D. Demadis, (Eds.) Royal Society of Chemistry, Cambridge, U.K., 2012, Chapter 14, pp. 438-492.
48 M. Taddei, F. Costantino, A. Ienco, A. Comotti, P.V. Dau, S.M. Cohen, M. *Chem. Commun.,* 2013, **49**, 1315−1317.
49 R.F. Mendes, D. Ananias, L.D. Carlos, J. Rocha, F.A. Almeida Paz, *Cryst. Growth Des.,* 2017, **17**, 5191-5199.
50 A.D.G. Firmino, F. Figueira, J.P.C. Tomé, F.A. Almeida Paz, J. Rocha, *Coord. Chem. Rev.*, 2018, **355**, 133–149.
51 APEX2 v2014.9-0, Bruker AXS Inc., Madison, WI, 2014.
52 A. Boultif, D. Louër, *J. Appl. Cryst.,* 2004, **37**, 724–731.
53 H.M. Rietveld, *J. Appl. Cryst.,* 1969, **2**, 65–71.
54 A.C. Larson, R.B. Von Dreele, *General Structure Analysis System (GSAS)*; Los Alamos National Laboratory Report LAUR 86-748, 2004.
55 winDETA; Novocontrol GmbH: Hundsangen, Germany, 1995.
56 D. Massiot, F. Fayon, M. Capron, I. King, S. Le Calvé, B. Alonso, J-O. Durand, B. Bujoli, Z. Gan, G. Hoatson, *Magn. Reson. Chem.* 2002, **40**, 70-76.
57 A. Moschona, N. Plesu, G. Mezei, A. Thomas, K.D. Demadis, *Corr. Sci.* **2018**, submitted for publication.
58 E. Akyol, M. Öner, E. Barouda, K.D. Demadis, *Cryst. Growth Des.,* 2009, **9**, 5145–5154.
59 M. Bazaga-García, M. Papadaki, R.M.P. Colodrero, P. Olivera-Pastor, E.R. Losilla, B. Nieto-Ortega, M.A.G. Aranda, D. Choquesillo-Lazarte, A. Cabeza, K.D. Demadis, *Chem. Mater.,* 2015, **27**, 424–435.
60 K.D. Demadis, M. Papadaki, I. Cisarova, I. *ACS-Appl. Mater. Interf.,* 2010, **2**, 1814–1816.
61 R.M.P. Colodrero, A. Cabeza, P. Olivera-Pastor, J. Rius, D. Choquesillo-Lazarte, J.M. García-Ruiz, M. Papadaki, K.D. Demadis, M.A.G. Aranda, *Cryst. Growth Des.,* 2011, **11**, 1713–1722.
62 K.D. Demadis, M. Papadaki, R.G. Raptis, H. Zhao, *J. Solid State Chem.,* 2008, **181**, 679-683.
63 K.D. Demadis, M. Papadaki, R.G. Raptis, H. Zhao, H. *Chem. Mater.,* 2008, **20***,* 4835-4846.

64 R.M.P. Colodrero, P. Olivera-Pastor, A. Cabeza, M. Papadaki, K.D. Demadis, M.A.G. Aranda, *Inorg. Chem.,* 2010, **49**, 761–768.
65 K.D. Demadis, S.D. Katarachia, *Phosphorus Sulfur Silicon,* 2004, **179**, 627-648.
66 K.D. Demadis, S.D. Katarachia, M. Koutmos, *Inorg. Chem. Commun.,* 2005, **8**, 254-258.
67 K.D. Demadis, S.D. Katarachia, H. Zhao, R.G. Raptis, P. Baran, *Cryst. Growth Des.,* 2006, **6**, 836-838.
68 L. Jiménez-García, A. Kaltbeitzel, V. Enkelmann, J.S. Gutmann, M. Klapper, K. Müllen *Adv. Funct. Mater.,* 2011, **21**, 2216–2224.
69 P. Colomban, *Proton Conductors: Solids, Membranes and Gels Materials and Devices.* Chemistry of Solid State Materials; Cambridge University Press: Cambridge, U.K., 1992; Vol. 2.
70 A. Florencia-Crespi, A. Jesús-Byrne, D. Vega, A. Karina-Chattah, G.A. Monti and J.M. Lázaro-Martínez *J. Phys. Chem. A* 2018, **122**, 601−609.
71 R.M.P. Colodrero, K.E. Papathanasiou, N. Stavgianoudaki, P. Olivera-Pastor, E.R. Losilla, M.A.G. Aranda, L. León-Reina, J. Sanz, I. Sobrados, D. Choquesillo-Lazarte, J.M. García-Ruiz, P. Atienzar, F. Rey, K.D. Demadis, A. Cabeza *Chem. Mater.,* 2012, **24**, 3780−3792.

TOC entry

A family of alkali metal-based frameworks containing the tetraphosphonate linker hexamethylenediamine-N,N,N′,N′-*tetrakis*(methylenephosphonic acid), HDTMP, exhibiting rich structural diversity, and water-dependent proton conductivity.